Heliyon 7 (2021) e08571

Contents lists available at ScienceDirect

Heliyon

journal homepage: www.cell.com/heliyon

Research article

Green synthesis of copper oxide nanoparticles using extracts of *Solanum macrocarpon* fruit and their redox responses on SPAu electrode

Enyioma C. Okpara [a,b], Oluwasayo E. Ogunjinmi [c], Opeyemi A. Oyewo [d], Omolola E. Fayemi [a,b], Damian C. Onwudiwe [a,b,*]

[a] *Material Science Innovation and Modelling (MaSIM) Research Focus Area, Faculty of Natural and Agricultural Sciences, North-West University (Mafikeng Campus), Private Bag X2046, Mmabatho, South Africa*

[b] *Department of Chemistry, School of Physical and Chemical Sciences, Faculty of Natural and Agricultural Science, North-West University (Mafikeng Campus), Private Bag X2046, Mmabatho, South Africa*

[c] *Industrial Chemistry Unit, Department of Physical Sciences, First Technical University, Ibadan, Oyo State, Nigeria*

[d] *Department of Science and Technology Education, Faculty of Education, University of Johannesburg, Johannesburg, South Africa*

HIGHLIGHTS

- CuO NPs were prepared using aqueous extracts of *Solanum macrocarpon* fruit.
- Both the conventional heating and microwave irradiationmethods were employed.
- The microscopic and structural properties of the NPs were studied and compared.
- The electrochemical activities of the CuO modified SPAu electrodes were investigated.
- The synthesis routes played a major role in the growth and applicability of the NPs.

GRAPHICAL ABSTRACT

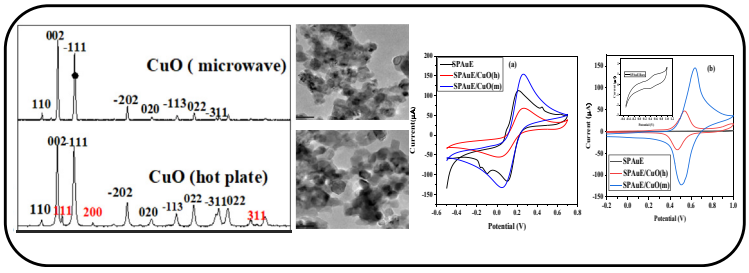

ARTICLE INFO

Keywords:
Green synthesis
Copper oxides
Solanum macrocarpon
Microwave irradiation
Redox behaviour

ABSTRACT

In this work, CuO nanoparticles (NPs) were prepared from the aqueous extracts of *Solanum macrocarpon* fruit by using the conventional heating (CuO(h) NPs) and microwave irradiation (CuO(m) NPs) methods. The synthesized nanoparticles were characterized using scanning electron microscopy (SEM), transmission electron microscopy (TEM), and X-ray diffraction (XRD). The SEM analysis revealed that the CuO NPs from both routes contained essentially smooth surfaces, and displayed some degree of agglomeration. The TEM analysis confirmed some spherical morphology with mean particle sizes of 35.60 ± 6.24 nm and 47.14 ± 6.18 nm for the CuO(h) and CuO(m) NPs respectively. While the CuO(m) NPs possessed a single-phase consistent with the face cantered cubic structure of copper oxide, the CuO(h) NPs showed some extra peaks attributed to Cu_2O NPs as secondary phase. Electrochemical studies were conducted in order to evaluate the electrochemical properties of the NPs. The responses of a gold screen-printed electrode surface treated with both NPs showed that their redox behaviours on $(Fe(CN)_6)^{3-/4-}$ probe and KCl electrolytes vary significantly. In $(Fe(CN)_6)^{3-/4-}$ probe, the SPAuE/CuO(h) showed enhanced electrochemical response relative to the bare, while the SPAuE/CuO(m) showed a lower current response than the bare. However, in the KCl electrolye, the SPAuE/CuO(h) and SPAuE/CuO(m) were highly electroactive and demonstrated peak current magnitude that was about 26.5 and 83.38 times higher than that of

* Corresponding author.
E-mail address: Damian.Onwudiwe@nwu.ac.za (D.C. Onwudiwe).

https://doi.org/10.1016/j.heliyon.2021.e08571
Received 14 October 2021; Received in revised form 11 November 2021; Accepted 6 December 2021

the bare. In this KCl medium, the magnitude of the oxidation peak current of Cu^{2+} for SPAuE/CuO(m) was about 3 times higher than that of SPAuE/CuO(h). The percentage contraction in redox coordinates between the 1st and 10th scans in both electrodes were 3.88 and 19.28% for SPAuE/CuO(h) and SPAuE/CuO(m) respectively. Thus, the choice of green synthesis route could be exploited in different fields where green NPs is desired.

1. Introduction

Copper oxides nanoparticles (CuO NPs) have found a broad range of applications in various areas such as drug delivery, biological activities (including antifungal, antibacterial, antioxidant agencies), generation of solar power, optics, sensors, and water purification methodologies [1, 2, 3, 4]. These wide spectra of applications stem from their unique properties such as high surface area, small particle size, non-toxicity, availability of precursor materials, and very low synthesis costs [5]. Consequently, research attention has lately been focused on different routes to the synthesis of CuO NPs. In previous study, the electrochemical properties of CuO NPs from waste biomass was used to modify the surface of a screen-printed carbon electrodes (SPCE). The modified electrodes showed well defined redox peaks, higher current response and electroactive areas relative to the bare SPCE [5].

Generally, NPs could be prepared using either the top-down, or bottom-up approach. These methods include the physical, chemical and biological methods [6, 7]. The chemical and physical methods include, chemical precipitation, sonochemical, single step-wet synthesis, thermal oxidation, sol-gel, solid thermal state decomposition, microwave irradiation, and laser ablation [8]. Although, these chemical and physical methods have been proven to be highly efficient in NPs synthesis, the setbacks associated with them cannot be overlooked. The chemical methods often involve the use and generation of toxic by-products, while the physical methods are intrinsically unsustainable. They are often very expensive, in addition to possible formation of surface structural imperfections [9, 10, 11, 12]. On the other hand, biological methods which involve the use of environmentally friendly, and low-cost biological materials such as different parts of plants, fungal, algae, bacterial, and actinomycetes species could be considered competitive alternative [13].

The ease, low cost, and speed of synthesis of the nanoparticles with extracts from different parts of plant have given them an edge over other biological entities [14, 15, 16]. Very stable nano scaled CuO particles have been successfully synthesized using various extracts from roots, leaves, fruits, peels, seeds, flowers, stems, and barks of plants [17]. The mixing of precursor materials with the aqueous extracts and thermal agitation of the solution using hotplates with magnetic stirrers is a common route to obtain the NPs using plant materials. Recently, the use of microwave irradiation in green synthesis of nanomaterials has proven to be efficient depending on the choice of plant extract [18, 19]. Although, several plant extracts have been used as a base material for the synthesis of CuO NPs, the use of extracts from *Solanum macrocarpon* fruit is yet to be explored in materials synthesis despite its unique properties.

Solanum is a well-known plant genus of the Solanaceae family, with more than 1000 species across the globe and not less than 100 species domicile in Africa and neighbouring islands [20]. *Solana macrocarpon,* which is also known as garden egg, is a common tropical specie and commonly cultivated in Africa. They are traditionally used as therapeutics against a wide range of ailments such as nasal infections, allergic rhinitis, asthma, rheumatic disease, diabetics, obesity, dyspepsia, bone joint swelling and pains, skin disease, gastro-oesophageal reflux disease. Also, *Solanum* fruits are very rich in various phytochemicals such as saponins, alkaloids, tannins, ascorbic acids and flavonoids [20]. Despite the abundant presence of these bioactive phytochemicals in this plant species, limited information is provided in the literature to describe the application of any part of garden egg in bio-synthesis of NPs.

Consequently, this work described the synthesis of CuO NPs from *Solanum macrocarpon* fruit using two different syntheses routes: the conventional boiling and microwave irradiation methods. The performance of screen plate gold electrode (SPAuE) modified with these CuO NPs and their electrochemical responses were investigated and compared. The physicochemical properties such as structure, crystallinity and particle size were also investigated by using XRD, SEM, and TEM in order to correlate these properties with the performance achieved during electrochemical response.

2. Materials and methods

2.1. Materials

Solanum macrocarpon fruits used were obtained from Ekiti, a South-Western state of Nigeria and were properly identified. Copper acetate monohydrate, potassium hexacyanoferrate (III), (K_3 $[Fe(CN)_6]$/potassium hexacyanoferrate (II), (K_4 $[Fe(CN)_6]$, dimethylsulfoxide (DMSO) and dimethylformamide (DMF) were purchased from Merck chemicals, South Africa. K_3 $[Fe(CN)_6]/K_4$ $[Fe(CN)_6]$ were used to prepare 10 mM $(Fe(CN)_6)^{3-/4-}$ at pH ≈ 7.2 and used as electrochemical probe containing 0.1 M KCl. Pure aqueous 0.1 M KCl (Metrohm, Switzerland) was used as the electrolyte. The deionized water used for the solution preparation in this study was produced by the Purite water system (Model Select Analyst HP40, United Kingdom). All chemicals used were of analytical grade. The disposable screen-printed electrode was obtained from Metrohm Cooperation, South Africa, consisting of 4 mm diameter gold working electrode, carbon counter electrode and a pseudo-silver reference electrode.

2.2. Methods

2.2.1. Extraction from Solanum macrocarpon fruits

The fresh fruits, Figure 1, were shredded, dried at room temperature and pulverized. About 5 g of the powder was then boiled for 2 h in 100 mL distilled water at 60 °C. The fruit extract was filtered through Whatman filter Paper No.1 and was stored in a refrigerator for further experiments.

2.2.2. Green synthesis of CuO nanoparticles using Solanum macrocarpon fruit extract

The synthesis of CuO nanoparticles involved two routes: thermal agitation by boiling and microwave irradiation, in order to take advantage of the possible changes that occurred in their chemical and physical properties for electrochemical response.

Figure 1. *Solanum macrocarpon* fruit.

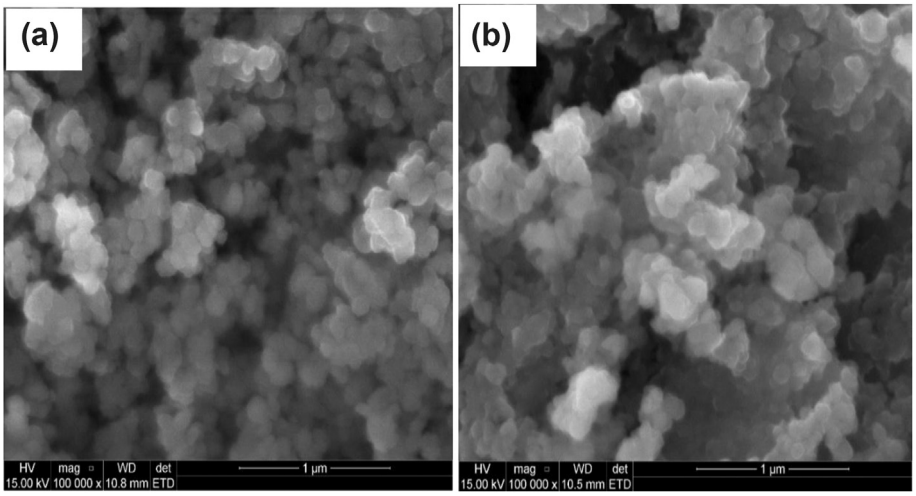

Figure 2. The SEM image of (a) CuO(h) NPs and (b) CuO(m) NPs.

2.2.2.1. Synthesis by conventional refluxing route. The details of this procedure has been reported elsewhere [21]. Briefly, 10 mL of *Solanum macrocarpon* fruit extract was stirred with 80 mL of 1 mM copper acetate solution in a 250 mL beaker. The pH of the mixture was adjusted to pH 7 using 0.1M of NaOH, and then heated up to 80 °C for 2 h. A colour change from green to dark brown was observed, which suggested the formation of copper oxide. The solution was allowed to cool down to room temperature and the brown precipitates were separated via centrifugation. The products were then doubled washed with distilled water to remove the unreacted reagents. The obtained product was oven-dried at 80 °C overnight, prior to calcination process in a furnace at 400 °C for 2 h to afford copper oxide nanoparticles denoted as CuO(h) NPs.

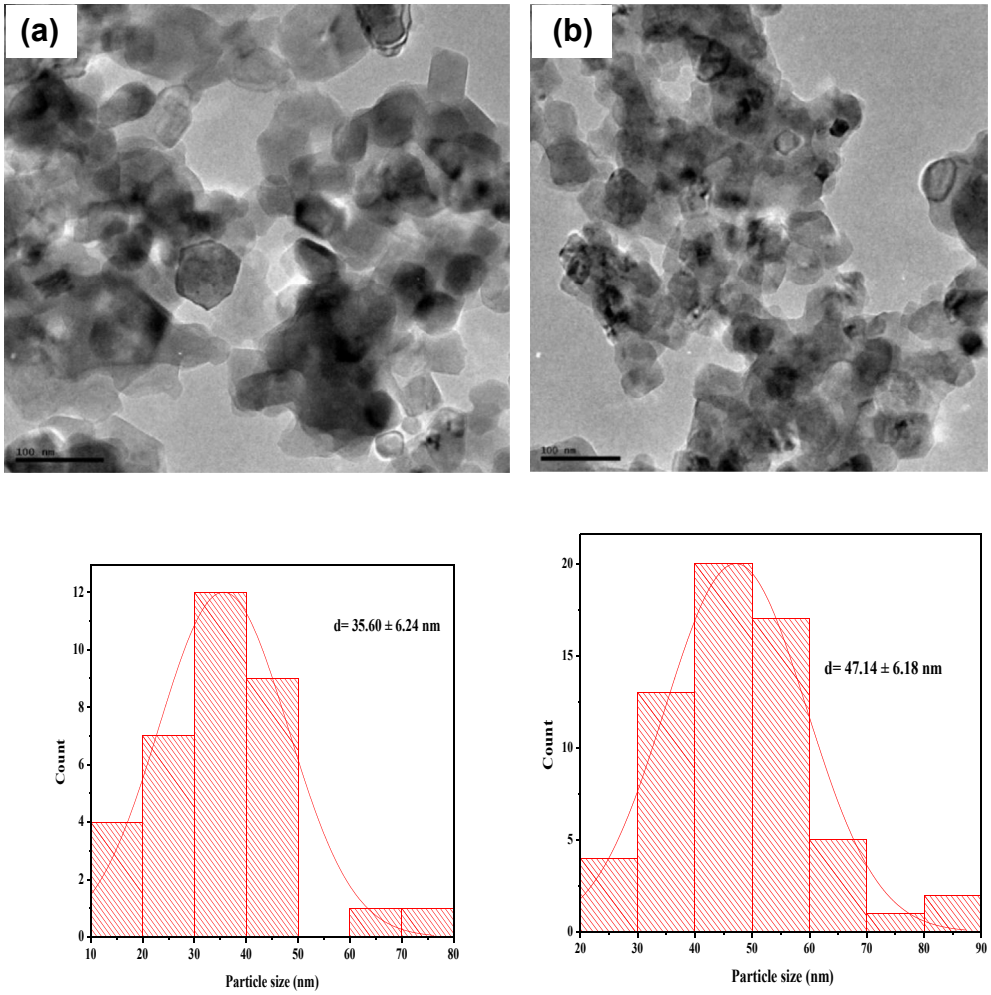

Figure 3. TEM images of (a) $CuO_{(h)}$, (b) $CuO_{(m)}$ NPs and their respective particle size distribution (c and d).

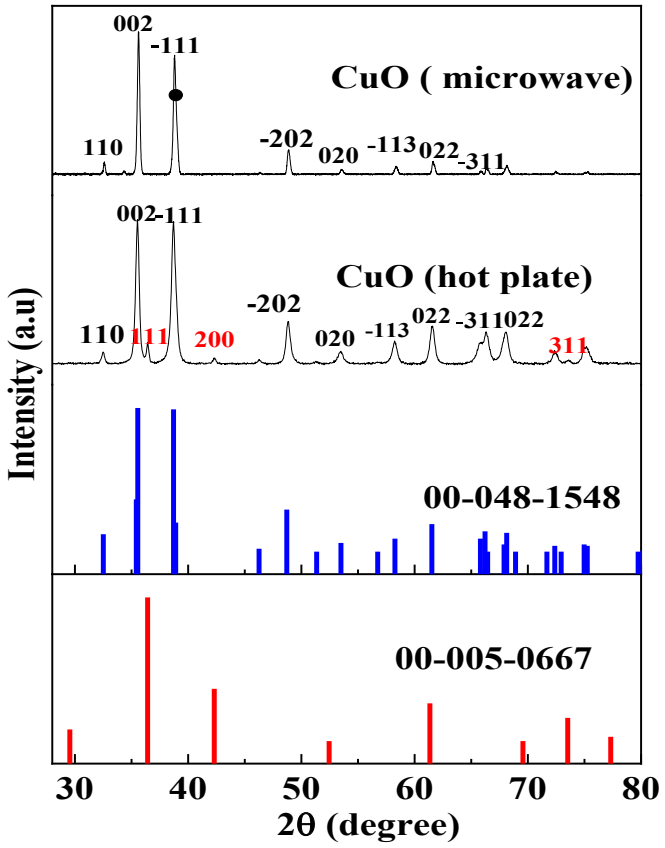

Figure 4. XRD patterns of copper oxide nanoparticles mediated by *Solana macrocarpon*.

2.2.2.2. Synthesis by microwave irradiation route. About 10 mL of *Solanum macrocarpon* fruit extract was added to 80 mL of 1 mM copper acetate solution in a 250 mL beaker. The mixture was stirred and the pH was adjusted to 7 by a dropwise addition of NaOH. The solution was then transferred to a Teflon lined microwave reactor vessel and then subjected to microwave irradiation operating at a power of 800 W for 1 h [22]. The resulting mixture was centrifuged and rinsed with distilled water to obtain the CuO(m) NPs.

2.2.3. Electrochemical studies

Gold-based screen-printed electrode (SPAuE) was treated with the as prepared NPs using drop cast method to obtain CuO(h) and CuO(m) NPs modified SPAuEs, which then referred to as SPAuE/CuO(h) and SPAuE/CuO(m) respectively. About 1.8 mg of the copper oxides NPs was measured into a glass tablet vial and 4–8 drops of a mixture of DMF and DMSO were added into the vial and sonicated to ensure even dispersion of the NPs in the solvents. About 20 μL each of the mixtures was then cast on the surface of the gold electrode to cover it fully and dried.

Cyclic voltammetry was used to study the redox behaviour of the bare and the modified Au electrodes in two different solutions with Metrohm 8400 series potentiostat software. The voltammetry conditions used were: a potential step of 2 mV, equilibrium time of 3 s, potential windows between -500 mV and +1000 mV, and all potentials were measured at Ag/AgCl. All experiments were performed at room temperature, assuming the temperature of 293 K. Each electrode was then washed sumptuously with distilled water before use and were reused where necessary.

3. Results and discussion

3.1. Morphology of the as prepared NPs

The Surface morphology of the CuO(h) NPs and CuO(m) NPs were investigated using scanning electron microscopy as presented in Figure 2 a and b. The as prepared CuO NPs show unevenly sized, smooth surfaced spherical morphologies in both cases. However, the CuO(m) NPs demonstrated larger particle size than the CuO(h) NPs. The rate of nucleation of the NPs in both routes was likely influenced by high temperature, and could be attributed to the product super saturation and accelerated core formation [23, 24]. The aggregation rate of the NPs might be the determinant factor for the structure and morphology of the NPs [25].

Figure 3 (a and b) presents the TEM images of the as-prepared CuO(h) and CuO(m) NPs respectively. Both samples showed irregular shaped particles. CuO(h) NPs consist of a mixture of hexagonal and spherical nanoparticles, while the CuO(m) NPs consist of mainly quasi-spherical particles. The difference in their morphology is related to the changes associated with synthesis approach. The particle size distribution histogram (Figure 3 c and d) demonstrated an increase in mean particle size from 35.60 ± 6.24 nm for CuO(h) NPs to 47.14 ± 6.18 nm for CuO(m) NPs.

3.2. X-ray diffraction studies

The crystalline phase of CuO(h) and CuO(m) NPs were studied using XRD analysis and the diffraction patterns are presented in Figure 4. The structure and composition of the CuO NPs are influenced by the various routes of bio-reduction employed. The diffraction peaks which appeared

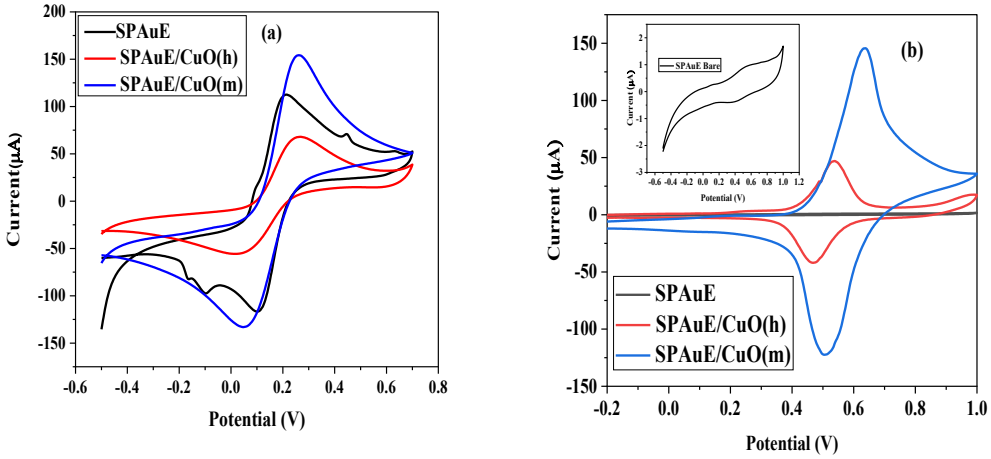

Figure 5. (a) The CV of the electrodes in 10 mM $(Fe(CN)_6)^{3-/4-}$ containing 0.1 M KCl at pH of ≈7.2 (b) the CV of the electrodes in 0.1 M KCl at 25 mV/s.

Table 1. The redox coordinates derived at the electrodes in $(Fe(CN)_6)^{3-/4-}$ at pH of ≈7.2 and KCl (pH = 6.4).

Electrode	Ip_a (μA)	Ep_a (V)	Ipc (μA)	E_{pc} (V)	I_{pa}/I_{pc}	ΔE (V)	I_m/I_b
$(Fe(CN)_6)^{3-/4-}$ containing 0.1 M KCl at 25 mV/s							
SPAuE	111.85	0.21	-116.70	0.10	0.96	0.11	1
SPAuE/CuO(h)	154.06	0.26	-133.22	0.05	1.16	0.21	1.4
SPAuE/CuO(m)	67.82	0.27	-56.15	0.01	1.21	0.26	0.6
0.1 M KCl at 25 mV/s							
SPAuE	1.78	0.56	-0.16	0.49	11.25	0.07	1
SPAuE/CuO(h)	47.22	0.53	-43.57	0.47	1.08	0.06	26.53
SPAuE/CuO(m)	148.42	0.63	-122.74	0.51	1.21	0.12	83.38

at 2θ degrees of approximately 32.50°, 35.52°, 38.71°, 48.83°, 53.50°, 58.23°, 61.59°, 66.33°, 67.98°, 68.08°, 72.37°, 75.01° and 75.18° were ascribed to the (110), (002), (−111), (−202), (020), (202), (−113), (022), (s), (220), (311), (004), and (−222) of the face-centered monoclinic CuO (JCPDS No. 00-048-1548) [26]. An insignificant average percentage contractions of the diffraction peaks (2θ) for CuO(h) and CuO(m) NPs from the JCPDS No. 00-048-1548 were 0.075% and 0.157% respectively. In addition, the diffraction pattern of CuO(h) NPs revealed additional diffraction peaks at 2θ = 29.56°, 36.42°, 42.30°, 52.46°, 61.35°, 69.57°, 73.53°, and 77.33° corresponding to (110), (111), (200), (211), (220), (310), (311) and (222) planes of cubic Cu_2O NPs (JCPDS No. 00-005-0667) [27]. This observed difference in phases confirm the dependence of the copper oxide phases on factors such as synthesis route, type of precursor used and synthesis temperature employed [28].

The calculated average crystalline sizes (D_v) using Debye-Scherrer's formula for CuO(h) NPs and CuO(m) NPs were found to be 19.08 ± 2.01nm and 32.06 ± 3.61nm respectively. This large variation in crystalline size is also evidenced by the broader diffraction peaks in CuO(h) NPs relative to the CuO(m) NPs. The crystalline sizes estimated using Debye-Scherrer's formula, differ from the average particle sizes obtained from TEM analysis. This could be attributed to the possibility of the TEM analysis to account for both crystalline and amorphous materials in the particles, while the XRD analysis accounts for only the crystalline domain of the NPs [29, 30].

3.3. Electrochemical characterization of the SPAuE/CuO NPs

The electrochemical characterization of the SPAu electrode modified with CuO NPs was examined using cyclic voltammetry in two different solutions; (1) 10 mM $(Fe(CN)_6)^{3-/4-}$ probe prepared in 0.1 M KCl and (2) 0.1 M KCl electrolyte. This is to understand the possible influence of ionic radicals contained in the probe on the redox current response of the electrodes. The electrochemical responses of the three working electrodes, bare SPAuE, SPAuE/CuO(h) and SPAuE/CuO(m) were examined. The redox responses of the electrodes in both solutions are represented in Figure 5. In the $(Fe(CN)_6)^{3-/4-}$ probe (Figure 5a), the bare SPAuE and the modified electrodes showed pronounced redox peaks that are characteristic of $(Fe(CN)_6)^{3-/4-}$ probe. The bare gold based SPE without modifications showed very high current response in the probe consequently, the use of very electroactive material is required to obtain enhanced redox response in the surface treatment.

As observed in Table 1, the magnitude of the oxidation peak current SPAuE/CuO(h) was 1.4 times higher than that of the bare SPAuE, while SPAuE/CuO(m) was lower than the bare by a factor of approximately equal to 0.6. A sharp contrast was observed in the redox responses of the three electrodes in 0.1 M KCl electrolyte, as presented in Figure 5b. The bare SPAuE displayed a very weak redox response, with no pronounced redox peaks coordinates (Figure 5b in set), while the modified electrodes showed well defined redox peaks at around potential range of 0.45–0.58 V. These redox peaks are attributed to the oxidation and reduction of Cu to Cu^{2+} and reduction of Cu^{2+} to Cu in the KCl medium. In addition, it is apparent that the SPAuE/CuO(m) with the lowest current response in the $(Fe(CN)_6)^{3-/4-}$ demonstrated the highest Cu^{2+} peak current magnitude in the KCl medium. Hence, the suppressed current response observed for SPAuE/CuO(m) could be attributed to the electrostatic repulsion between the positive ions of $Fe^{2+/3+}$ in the $(Fe(CN)_6)^{3-/4-}$ probe and the highly electroactive Cu^{2+} radical of CuO(m) NPs [31, 32]. Similar observation has been reported in studies related to $(Fe(CN)_6)^{3-/4-}$ probe [33, 34, 35].

Additionally, the magnitude of the peak to peak potential separation (ΔEp) for the bare and modified electrodes in both $(Fe(CN)_6)^{3-/4-}$ and KCl media, was more than 59 mV (a theoretical value for a perfect redox system), while the redox peak ratios showed deviation from unity (Table 1). This suggests that the redox behaviours of the electrodes in both solutions are characteristic of a quasi-reversible system (25 mV/s scan rate) [31]. However, in KCl media, the peak to peak separations (ΔEp) for both electrodes were less in magnitude compared to that of the $(Fe(CN)_6)^{3-/4-}$, and further confirms the removal of the electrostatic repulsive effect in $(Fe(CN)_6)^{3-/4-}$ media.

3.3.1. Scan rate study

Figure 6 displayed a number of voltammograms at different scan rates generated for the three electrodes in the $(Fe(CN)_6)^{3-/4-}$ probe containing 0.1 M KCl, and 0.1 M KCl electrolyte. The scan rate of the bare SPAu electrode continued to increase from 10 to 175 mV/s (Figure 6a), while that of the modified electrodes increased up to 200 mV/s in $(Fe(CN)_6)^{3-/4-}$ probes (Figure 6b and c). The redox potential in all the electrodes shifted to the right at the anode and to the left at the cathode with increase in the scan rate. The peak-peak potential separation (ΔEp) increased also with increase in the scan rate (Figure 6d inset). There was an increase from 79.2 mV to 127. 6 mV for the scan rate of 10 mV/s to 175 mV/s, 213. 3 mV to 378.4, and 157.5 mV–527.7 mV/s at the scan rate of 10 mV/s to 200 mV/s for the bare, SPAuE/CuO(h), and SPAuE/CuO(m) respectively. The ΔEp, was broader in the SPAuE/CuO(h), and SPAuE/CuO(m), which could be attributed to ohmic drop or slower rate of electron transfer in the $(Fe(CN)_6)^{3-/4-}$ medium [31]. Also, the redox peak current ratios increased with an increase in scan rate as shown in Figure 6d.

Similar redox responses are noticeable for the modified electrodes in KCl media Figure 6 (e and f). The potential peaks continued to shift to the right at the anode, while the cathodic peak potentials shifted to the left with an increase in scan rate. The redox peak coordinates continued to increase from the scan rate of 10 mV–225 mV/s. The magnitude of ΔEp increased from 50 mV to 200 mV, and 80 mV–460 mV at this range of scans. This is a considerate drop from the value of ΔEp obtained from the $(Fe(CN)_6)^{3-/4-}$ media which confirms the removal of the electrostatic repulsion offered by the $Fe^{2+/3+}$.

The peak redox coordinates in the probe solution, at different scan rates were recorded for the three electrodes. The plot of the anodic and cathodic peak currents against the square root of the scan rates (25 mV/s and above) represented a linear relationship (Figure 7) in all cases. This is an indication that the redox system is a diffusion-controlled process in the $(Fe(CN)_6)^{3-/4-}$ probe. Furthermore, a similar linear variation was observed in the plot of redox peak currents versus the scan rate

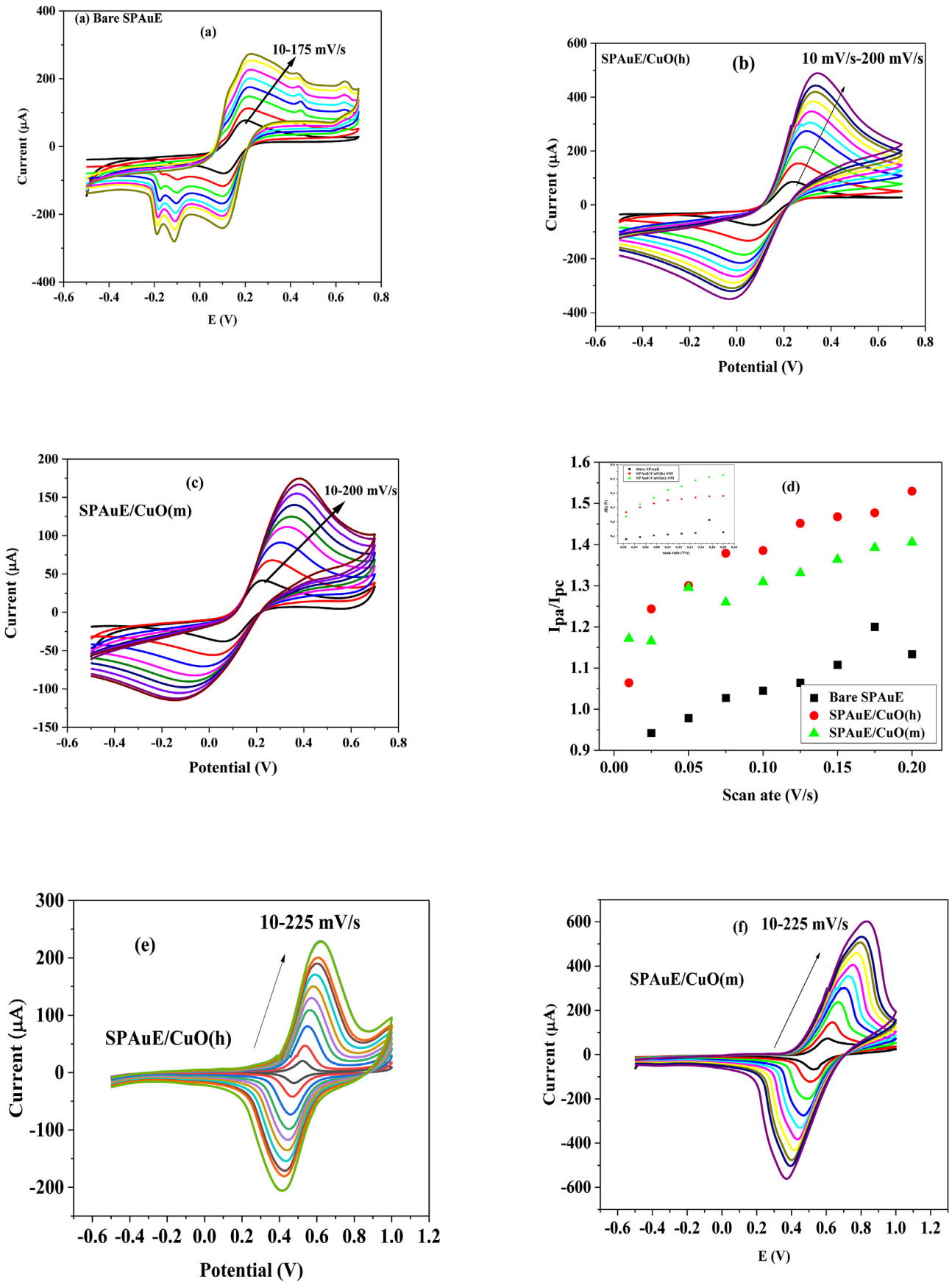

Figure 6. The variation of the redox cordinates with scan rate for (a) Bare in $(Fe(CN)_6)3^{-/4-}$, (b) SPAuE/CuO(h) in $(Fe(CN)_6)^{3-/4-}$, (c) SPAuE/CuO(m) in $(Fe(CN)_6)^{3-/4-}$ (d) Redox peaks variation with scan rate (inset: ΔEp with scan rate) in $(Fe(CN)_6)^{3-/4-}$ (e) SPAuE/CuO(h) in KCl, and (f) SPAuE/CuO(m) in KCl.

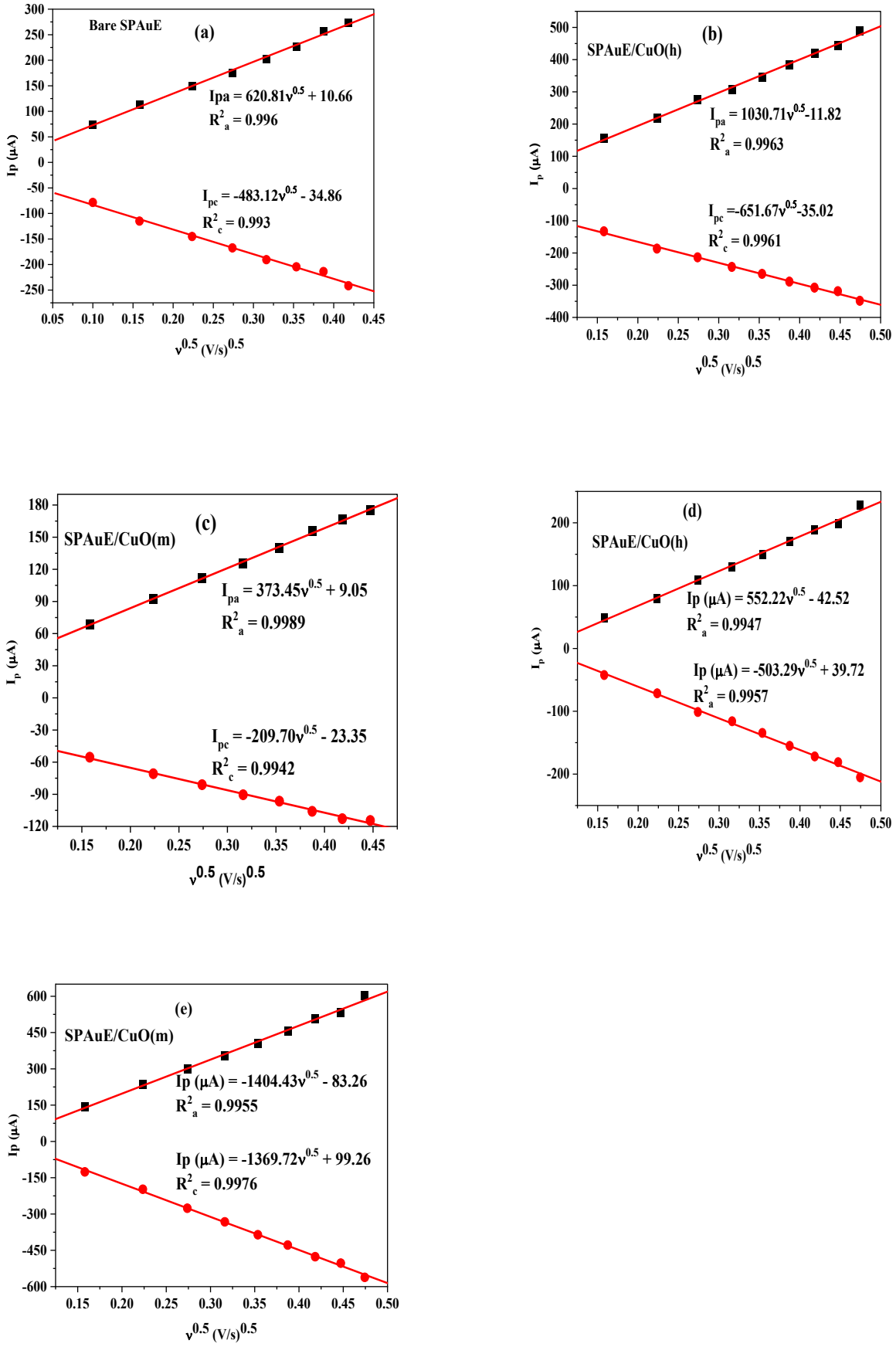

Figure 7. The plot of the linear variation of the peak current with square root of scan rate for (a) Bare in $(Fe(CN)_6)^{3-/4-}$, (b) SPAuE/CuO(h) in $(Fe(CN)_6)^{3-/4-}$ (c) SPAuE/CuO(m) in $(Fe(CN)_6)^{3-/4-}$, (d) SPAuE/CuO(h) in KCl, and (e) SPAuE/CuO(m) in KCl.

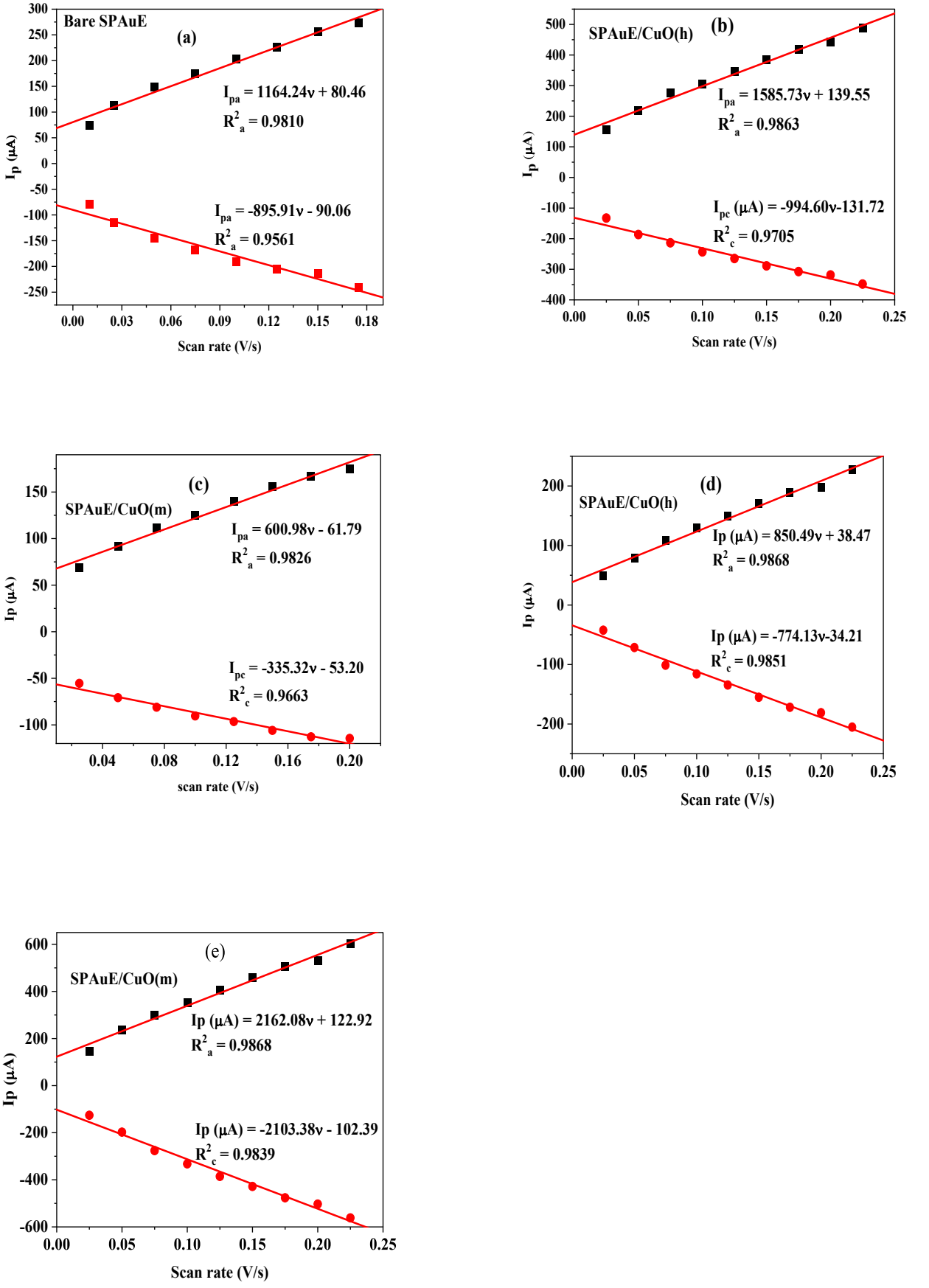

Figure 8. The plot of the linear variation of the peak current with scan rate for (a) Bare in $(Fe(CN)_6)^{3-/4-}$, (b) SPAuE/CuO(h) in $(Fe(CN)_6)^{3-/4-}$, (c) SPAuE/CuO(m) in $(Fe(CN)_6)^{3-/4-}$, (d) SPAuE/CuO(h) in KCl, and (e) SPAuE/CuO(m) in KCl.

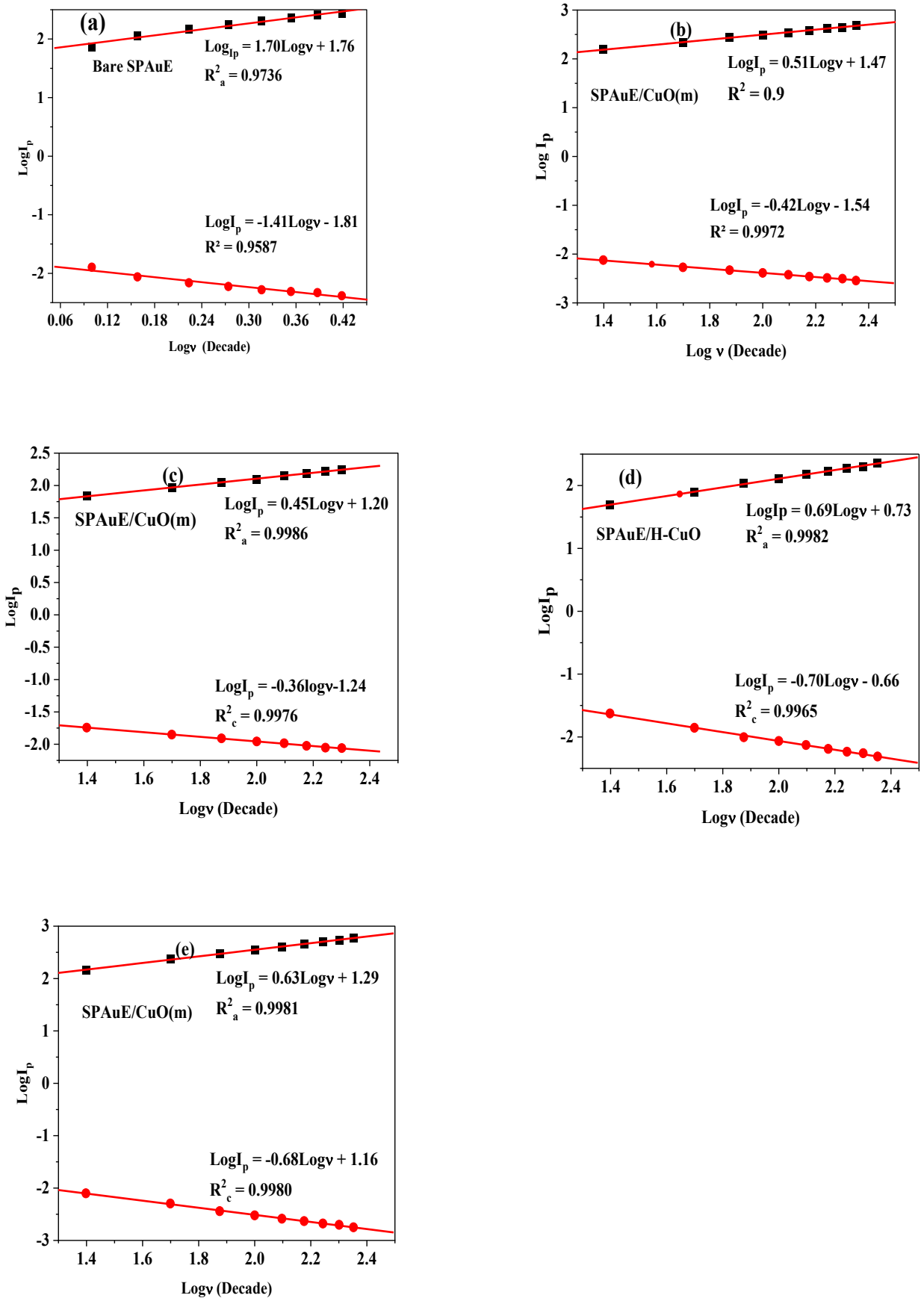

Figure 9. The plot of the linear variation of the log of peak current with log of scan rate for (a) Bare in $(Fe(CN)_6)^{3-/4-}$, (b) SPAuE/CuO(h) in $(Fe(CN)_6)^{3-/4-}$ (c) SPAuE/CuO(m) in $(Fe(CN)_6)^{3-/4-}$, (d) SPAuE/CuO(h) in KCl, and (e) SPAuE/CuO(m) in KCl.

Table 2. The rate transfer variables derived at the electrodes.

Electrode	n	α	nα	(1-α)	n (1-α)	k_s (s^{-1})	s	b (V/dec)
In $(Fe(CN)_6)^{3-/4-}$ probe								
SPAu	1.59	0.64	0.81	0.36	0.57	0.2208	1.7	0184
SPAuE/CuO(h)	1.2	0.5	0.6	0.5	0.60	0.0489	0.51	0.180
SPAuE/CuO(m)	0.68	0.38	0.26	0.62	0.42	0.0672	0.45	0.260
In 0.1 M KCl electrolyte								
SPAuE/CuO(h)	1.75	0.62	1.08	0.38	0.65	0.2529	0.69	0.160
SPAuE/CuO(m)	0.64	0.60	0.38	0.4	0.23	0.1436	0.63	0.410

s: slope of $LogI_p$ vs Log υ.

(Figure 8), which confirms that the process is a quasi-reversible diffusion and surface-controlled system. The peak current of the species adsorbed and desorbed is proportional to the scan rate (υ) and the square root of the scan rate ($\upsilon^{1/2}$) [36]. This is supported by the values of the anodic slopes (s) in the plot of $LogI_p$ vs Logυ (Figure 9), found to be 1.7, 0.51 and 0.45 for the bare, SPAuE/CuO(h) and SPAuE/CuO(m) respectively. For a diffusion-controlled process, the value of s ranges from 0 to 0.5; for a combination of both diffusion and surface control, the values of s ranges from 0.5-1.0, while for a sole surface controlled redox system, the ideal value of s is 1 [37]. Therefore, the modified electrodes were essentially diffusion controlled, which is a more desirable redox system.

In the KCl media, the oxidative and reductive peak of currents for the $Cu^{2+/}Cu^0$ were also recorded at different scan rates (10–225 mV/s) for the two modified electrodes and the plots of the redox coordinates were also generated (Figure 8). A linear variation was noticed in the relationship between the redox peak currents generated by the absorbed and desorbed Cu^{2+} and the scan rates in the KCl media (Figure 8 (d and e). A similar linear variation of the plot of the redox peak currents and the square root of the scan rate (Figure 7 (d and e)) was also recorded. The value of the slopes (s) of the linear plot of $LogI_p$ vs Logυ (Figure 9 (d and e) support that the system is a combination of both diffusion and surface controlled. At the bare, the SPAuE/CuO(h) and SPAuE/CuO(m) values of s realized were found to be 0.69 and 0.63 respectively.

3.3.2. Rate of transfer

The rate of transfer of electrons through the electrolyte in the interface between the electrode and the solution is very crucial in electrochemistry. Using the data generated from the CV, the rate transfer constants (k_s), and the charge transfer coefficients, which are highly dependent on electrode materials for a heterogeneous redox couple were computed (Table 2) [38].

$$\log ks = \alpha\log(1-\alpha) + (1-\alpha)\log\alpha - \log RT/nF\nu - \alpha(1-\alpha)nF\Delta Ep/RT \quad (1)$$

In the $(Fe(CN)_6)^{3-/4-}$ media, the theoretical values of α computed were 0.64, 0.5 and 0.38 for the bare, SPAuE/CuO(h), and SPAuE/CuO(m) respectively, while the value of $n\alpha_n$ were computed to be 0.81, 0.6 and 0.26 respectively. On the other hand, the value of the oxidation properties of the rate transfer coefficient, n (1-α), computed at the bare, SPAuE/CuO(h), and SPAuE/CuO(m) electrodes were found to be 0.57, 0.60 and 0.42 respectively. Given the values of n (1-α), the electron transfer at the anode was fastest in the SPAuE/CuO(h), followed by the bare SPAu and then SPAuE/CuO(m), which has been consistent with the trend of the redox behaviours observed in the three electrodes. The values of *ks* (Equation 1) computed were 0.22, 0.049 and 0.067 s^{-1} ((using a scan rate of 25 mV/s) at the bare SPAuE, SPAuE/CuO(h) and SPAuE/CuO(m) respectively. This lower value of the *ks* in both modified electrodes confirms the probabilities of ohmic potential drop (iRs) and slower transfer of electrons at the solution interface.

However, in the KCl medium, without a competitive like-ions and concomitant electrostatic repulsion, the value of *ks* for redox couple of the Cu^{2+} were evaluated. The computed values of *ks* were 0.25 s^{-1} and 0.14 s^{-1} at SPAuE/CuO(h) and SPAuE/CuO(m) respectively (using a scan rate of 25 mV/s) suggesting that, in the KCl medium, the rate of transfer of electron was very fast, supported by high current response and lower peak-peak redox potential separation (ΔEp).

A linear relationship was also observed in the plot of peak potential against the log of scan rate (Figure 10). Given that Ep (V) = b/2Logυ + c, (where b is the Tafel value), the slope of the plot of Ep vs Logυ was used to calculate the values of b [38]. In the $(Fe(CN)_6)^{3-/4-}$ medium, the values of b computed for the bare was, 0.188 V/dec, 0.26 V/dec, and 0.180 V/dec respectively. These are all higher than the theoretical value of 0.120 V/dec, for a one step and one electron redox process. This high value could be attributed to adsorption or the interference of reaction intermediates on the electrodes' surface. In the KCl medium, the value of b computed was 0.16 V/dec and 0.410 V/dec for SPAuE/CuO(h), and SPAuE/CuO(m) respectively. In this media, the Tafel slope value was far lower at the SPAuE/CuO(h), than the counterpart SPAuE/CuO(m). Theoretically, the Tafel slope (b) demonstrates how effectively an electrode can produce current in response to change in applied potential. Therefore, a lower value of b at the SPAuE/CuO(h) in the KCl medium means less over potential is required to get a high current response. This superior performance of this SPAuE/CuO(h) electrode, could be attributed to the smaller particle size, and less agglomeration of the CuO(h) NPs, in comparison with the CuO(m) NPs.

3.3.3. Stability of the electrodes

The stability of the bare and modified electrodes was examined by running 10 consecutive scans at a scan rate of 50 mV/s in 0.1M KCl medium (Figure 11). The SPAuE/CuO(h) was very stable, with an overall 3.88 % contraction in redox coordinates between the 1^{st} and 10^{th} scans (Table 3). On the contrary, the overall contraction in the redox coordinates between the 1^{st} and 10^{th} scans for the SPAuE/CuO(m) was about 19.28%. The contraction in the stability between the two electrodes could be attributed to differences in the particle sizes of the as-prepared CuO-NPs.

4. Conclusion

Nano dimensioned crystalline CuO nanoparticles were successfully synthesized using extracts from *Solanum macrocarpon* fruits via two routes: conventional heating method, and microwave irradiation method. The crystalline structures of the NPs were confirmed by XRD, which showed diffraction planes corresponding to the monoclinic CuO structure for the samples prepared from both routes, and additional secondary reflections corresponding to the cuprite (Cu_2O) structure in the pattern of the samples prepared using the conventional heating approach. This indicated that the microwave irradiation method is a better approach to purer sample in the reported study. The SEM micrographs showed that nanoparticles from both routes had smooth surfaced agglomerates, which were largely spherical in shape. However, TEM analysis showed that the NPs obtained by normal heating on the hotplate (CuO(h)) were smaller in size compared to the nanoparticles obtained via microwave irradiation. The surface of gold-based screen-printed electrodes modified with the as-prepared NPs was electrochemically

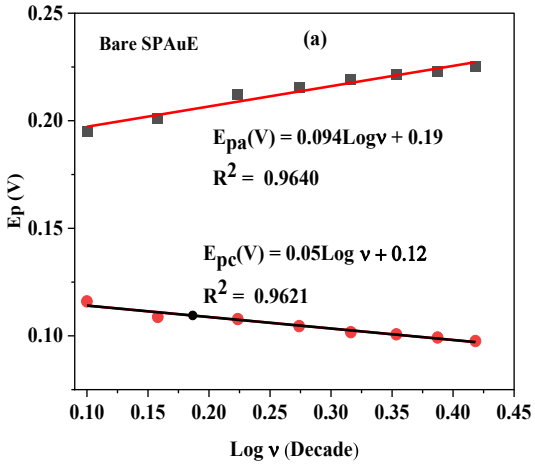

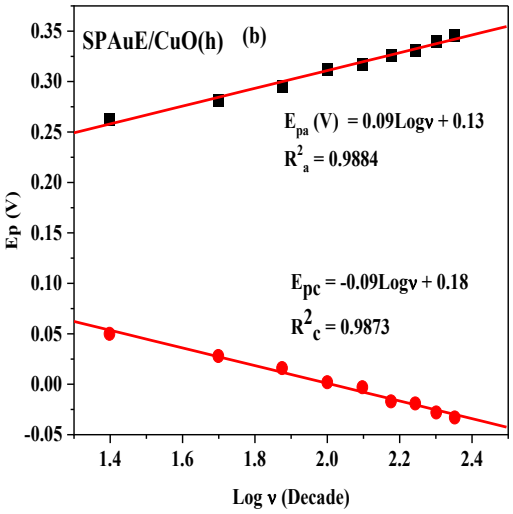

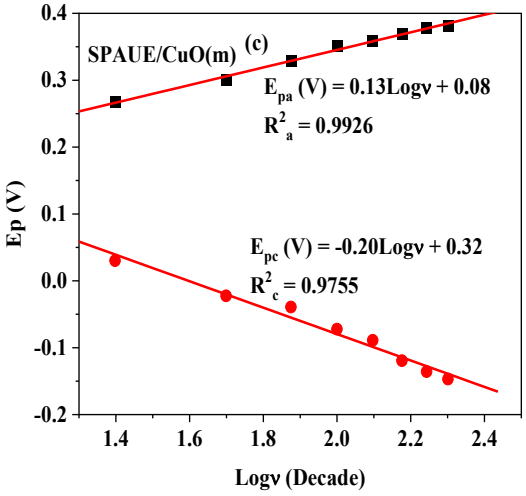

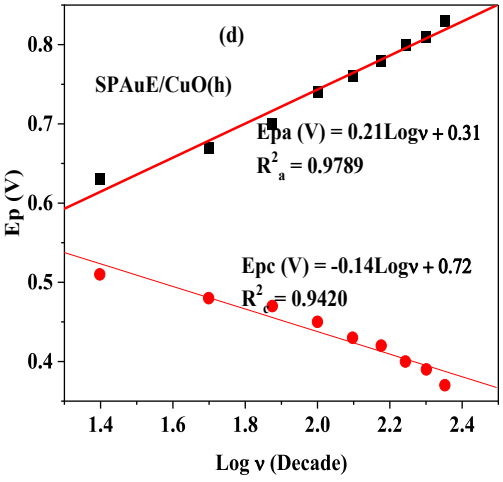

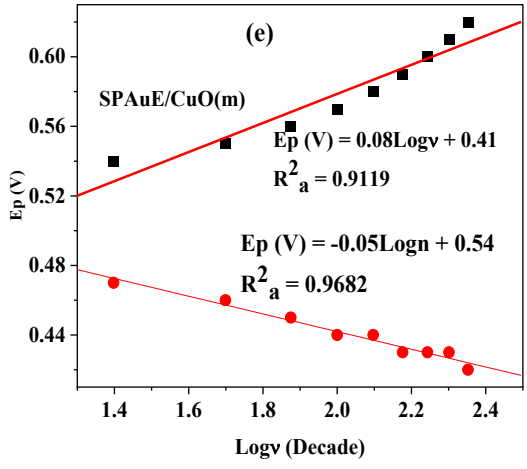

Figure 10. The plot of the linear variation of the peak voltage with log of scan rate for (a) Bare in $(Fe(CN)_6)^{3-/4-}$, (b) SPAuE/CuO(h) in $(Fe(CN)_6)^{3-/4-}$ (c) SPAuE/CuO(m) in $(Fe(CN)_6)^{3-/4-}$, (d) SPAuE/CuO(h) in KCl, and (e) SPAuE/CuO(m) in KCl.

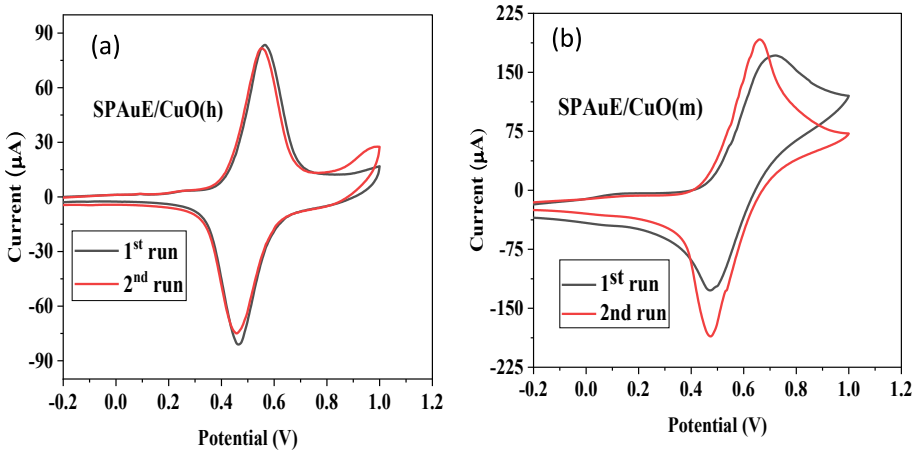

Figure 11. The stability of the electrodes in KCl for (a) SPAuE/CuO(h) and (b) SPAuE/CuO(m) (scan rate of 50 mV/s, pH = 6.4).

Table 3. The percentage contraction in the redox coordinates between the 1st and 10th scans for the three working electrodes.

Electrodes	I_{pa1}	I_{pa10}	% div.	I_{pc1}	I_{pc10}	% div.	E_{pa1}	Ep_{a10}	% div.	Ep_{c1}	Ep_{c10}	% div.	Total % div.
SPAuE	0.93	0.88	4.25	-0.89	-0.87	1.1	0.23	0.23	0.00	0.05	0.05	0.00	2.69
SPAuE/CuO(h)	83.55	81.54	2.41	-80.47	74.94	7.45	0.57	0.55	3.51	0.47	0.46	2.13	3.88
SPAuE/CuO(m)	186.66	191.33	11.11	-126.08	-186.66	32.45	0.72	0.66	14.29	0.47	0.47	0.00	19.28

% div.: % contraction between the first and tenth scans.

characterized using cyclic voltammetry. The redox responses showed that while the as-prepared SPAuE/CuO(h), and SPAuE/CuO(m) were very electroactive, their redox activities were highly dependent on the dimensions of the NPs and also the degree of agglomeration. Hence, the CuO (h) NPs with smaller dimensions and lesser agglomerations showed better electroactivity in the probe and electrolyte media investigated.

Declarations

Author contribution statement

Enyioma C. Okpara: Performed the experiments; Analyzed and interpreted the data; Wrote the paper.

Oluwasayo E. Ogunjinmi, Opeyemi A. Oyewo: Performed the experiments; Analyzed and interpreted the data.

Omolola E. Fayemi: Contributed reagents, materials, analysis tools or data.

Damian C. Onwudiwe: Contributed reagents, materials, analysis tools or data; Wrote the paper.

Funding statement

This research did not receive any specific grant from funding agencies in the public, commercial, or not-for-profit sectors.

Data availability statement

Data will be made available on request.

Declaration of interests statement

The authors declare no competing interests.

Additional information

No additional information is available for this paper.

References

[1] L. Zhang, et al., Nanoparticles in medicine: therapeutic applications and developments, Clin. Pharmacol. Therapeut. 83 (5) (2008) 761–769.
[2] Ç. Oruç, A. Altındal, Structural and dielectric properties of CuO nanoparticles, Ceram. Int. 43 (14) (2017) 10708–10714.
[3] R. Yathisha, et al., Study on the effect of Zn2+ doping on optical and electrical properties of CuO nanoparticles, Phys. E Low-dimens. Syst. Nanostruct. 108 (2019) 257–268.
[4] M.E. Grigore, et al., Methods of synthesis, properties and biomedical applications of CuO nanoparticles, Pharmaceuticals 9 (4) (2016) 75.
[5] E.C. Okpara, O.E. Fayemi, Comparative study of spectroscopic and cyclic voltammetry properties of CuONPs from citrus peel extracts, Mater. Res. Express 6 (10) (2019) 105056.
[6] M. Yadi, et al., Current developments in green synthesis of metallic nanoparticles using plant extracts: a review, Artif. Cells Nanomed. Biotechnol. 46 (sup3) (2018) S336–S343.
[7] P.G. Jamkhande, et al., Metal nanoparticles synthesis: an overview on methods of preparation, advantages and disadvantages, and applications, J. Drug Deliv. Sci. Technol. 53 (2019) 101174.
[8] A. Azam, et al., Size-dependent antimicrobial properties of CuO nanoparticles against Gram-positive and-negative bacterial strains, Int. J. Nanomed. 7 (2012) 3527.
[9] K.N. Thakkar, S.S. Mhatre, R.Y. Parikh, Biological synthesis of metallic nanoparticles, Nanomed. Nanotechnol. Biol. Med. 6 (2) (2010) 257–262.
[10] S. Kaabipour, S. Hemmati, A review on the green and sustainable synthesis of silver nanoparticles and one-dimensional silver nanostructures, Beilstein J. Nanotechnol. 12 (1) (2021) 102–136.
[11] A.Y. Ghidan, T.M. Al-Antary, A.M. Awwad, Green synthesis of copper oxide nanoparticles using Punica granatum peels extract: effect on green peach Aphid, Environ. Nanotechnol. Monit. Manag. 6 (2016) 95–98.
[12] R. Jagessar, Plant Extracts Based Nanoparticles, a Good Perspective in the Development of Drugs in Nanomedicine, 2020.
[13] K. Parveen, V. Banse, L. Ledwani, Green synthesis of nanoparticles: their advantages and disadvantages, in: AIP Conference Proceedings, AIP Publishing LLC, 2016.
[14] N. Pantidos, L.E. Horsfall, Biological synthesis of metallic nanoparticles by bacteria, fungi and plants, J. Nanomed. Nanotechnol. 5 (5) (2014) 1.
[15] N.A.N. Mohamad, et al., Plant extract as reducing agent in synthesis of metallic nanoparticles: a review, in: Advanced Materials Research, Trans Tech Publ, 2014.
[16] M. Ovais, et al., Green synthesis of silver nanoparticles via plant extracts: beginning a new era in cancer theranostics, Nanomedicine 12 (23) (2016) 3157–3177.
[17] H.N. Cuong, et al., New Frontiers in the Plant Extract Mediated Biosynthesis of Copper Oxide (CuO) Nanoparticles and Their Potential Applications: A Review, Environmental Research, 2021, p. 111858.
[18] G.T. Anand, et al., Microwave assisted green synthesis of CuO nanoparticles for environmental applications, Mater. Today Proc. 36 (2021) 427–434.
[19] I. Jahan, F. Erci, I. Isildak, Facile microwave-mediated green synthesis of non-toxic copper nanoparticles using Citrus sinensis aqueous fruit extract and their antibacterial potentials, J. Drug Deliv. Sci. Technol. 61 (2021) 102172.

[20] S.N. Chinedu, et al., Proximate and phytochemical analyses of Solanum aethiopicum L. and Solanum macrocarpon L. fruits, Res. J. Chem. Sci. 1 (3) (2011) 63–71.
[21] S. Sathiyavimal, et al., Green chemistry route of biosynthesized copper oxide nanoparticles using Psidium guajava leaf extract and their antibacterial activity and effective removal of industrial dyes, J. Environ. Chem. Eng. 9 (2) (2021) 105033.
[22] A. Saranya, et al., Facile one pot microwave-assisted green synthesis of Fe2O3/Ag nanocomposites by phytoreduction: potential application as sunlight-driven photocatalyst, antibacterial and anticancer agent, J. Photochem. Photobiol., B 207 (2020) 111885.
[23] N.T. Thanh, N. Maclean, S. Mahiddine, Mechanisms of nucleation and growth of nanoparticles in solution, Chem. Rev. 114 (15) (2014) 7610–7630.
[24] H. Liu, et al., Effect of temperature on the size of biosynthesized silver nanoparticle: deep insight into microscopic kinetics analysis, Arabian J. Chem. 13 (1) (2020) 1011–1019.
[25] D. Onwudiwe, et al., Hexavalent Chromium Reduction by ZnO, SnO2 and ZnO-SnO2 Synthesized Using Biosurfactants from Extract of Solanum Macrocarpon, 2021.
[26] H.J. Jung, Y. Yu, M.Y. Choi, Facile preparation of Cu2O and CuO nanoparticles by pulsed laser ablation in NaOH solutions of different concentration, Bull. Kor. Chem. Soc. 36 (2015) 3–4.
[27] L. Dahonog, M.D.D. Vega, M. Balela, pH-dependent synthesis of copper oxide phases by polyol method, in: Journal of Physics: Conference Series, IOP Publishing, 2019.
[28] M. Akhtar, et al., Phase controlled synthesis of copper sulfide nanoparticles by colloidal and non-colloidal methods, Mater. Chem. Phys. 180 (2016) 404–412.
[29] P. Lu, et al., Characterization of titanium dioxide and zinc oxide nanoparticles in sunscreen powder by comparing different measurement methods, J. Food Drug Anal. 26 (3) (2018) 1192–1200.
[30] A.A. Badawy, et al., Efficacy assessment of biosynthesized copper oxide nanoparticles (cuo-nps) on stored grain insects and their impacts on morphological and physiological traits of wheat (triticum aestivum l.) plant, Biology 10 (3) (2021) 233.
[31] A. Pendse, et al., Charged layered boron nitride-nanoflake membranes for efficient ion separation and water purification, Small 15 (49) (2019) 1904590.
[32] N. Ferreyra, L. Coche-Guérente, P. Labbé, Construction of layer-by-layer self-assemblies of glucose oxidase and cationic polyelectrolyte onto glassy carbon electrodes and electrochemical study of the redox-mediated enzymatic activity, Electrochim. Acta 49 (3) (2004) 477–484.
[33] V. Molinero, E.J. Calvo, Electrostatic interactions at self assembled molecular films of charged thiols on gold, J. Electroanal. Chem. 445 (1-2) (1998) 17–25.
[34] V. Pardo-Yissar, et al., Layered polyelectrolyte films on Au electrodes: characterization of electron-transfer features at the charged polymer interface and application for selective redox reactions, Langmuir 17 (4) (2001) 1110–1118.
[35] T.R. Farhat, J.B. Schlenoff, Ion transport and equilibria in polyelectrolyte multilayers, Langmuir 17 (4) (2001) 1184–1192.
[36] F. Haque, et al., A cyclic voltammetric study of the redox reaction of Cu (II) in presence of ascorbic acid in different pH media, Dhaka Univ. J. Sci. 61 (2) (2013) 161–166.
[37] W. Sun, M. Yang, K. Jiao, Electrochemical behaviors of neutral red on single and double stranded DNA modified electrode, Int. J. Electrochem. Sci. 2 (2007) 93–101.
[38] E.C. Okpara, et al., Green wastes mediated zinc oxide nanoparticles: synthesis, characterization and electrochemical studies, Materials 13 (19) (2020) 4241.